

HOLES

5.1 INTRODUCTION

We have already encountered holes in the Case 1 of the first map family treated at the end of the preceding chapter (see Fig. 4-17). We now change the parameter a from 0.7 to 1.0, obtaining Case 2 of the first map family, in which the bifurcations involving holes are somewhat clearer. This change eliminates the repelling 2-cycle, $\{Q_1, Q_2\}$. As before, the fixed point Q becomes a repelling focus, but the fixed point P is now a saddle.¹

The main qualitative features in the portrait of the iterations in this case are: a bounded absorbing area, d' , its basin of attraction, $D(d')$, the basin of attraction of infinity, $D(\infty)$, and the boundary between these two basins, F , which consists of the saddle P and its inset.

As the parameter b decreases from zero, the fixed point Q becomes a repelling focus, giving rise to an attractive closed invariant curve, Γ , as before. As Γ crosses L_{-1} there are several bifurcations and an annular absorbing area is obtained, bounded by a finite number of critical arcs, as before. Inside this annular absorbing area, a chaotic area appears.

1. See Figs. 3-4 to 3-8 to recall the meaning of these terms.

5.2 EXEMPLARY BIFURCATION SEQUENCE

In this chapter we present a very informative bifurcation sequence, including some new phenomena, ideas and observations. We discuss some of these events now, as b decreases from 0.593 to 0.600. We proceed in eleven stages.

Stage 1: $b = -0.59300$

Using Procedure 2 as in the previous chapter, we find an absorbing area d' , bounded by seven images of the straight line segment $b_0 a_0$ of L_{-1} . This is the shaded area in Fig. 5-1. Note that the boundary of d' includes arcs of L_5 and L_6 .

Inside d' there is also an attracting chaotic area, d , as shown in Fig. 5-2. Within d' there is an annular absorbing area d'_a , which contains d , and is bounded by the iterates of the line segment $a_0 b_0$ of L_{-1} shown in Fig. 5-1. This absorbing area is shown in Fig. 5-3, an enlargement is shown in Fig. 5-4.

These critical arcs also define the boundary of the chaotic attractor, shown in Fig. 5-5 as a densely dotted region. Note that the boundaries of d'_a and d include arcs of L_9 and L_{10} , as shown in Fig. 5-4, and in fact the entire boundary of d may be defined by critical arcs.

The basin of attraction $D(d')$ is shown in Fig. 5-6, in which the gray region denotes the basin of infinity, $D(\infty)$. The boundary between these two basins, F , is smooth, and consists of the inset of the fixed saddle point, P .

Note the corners of the arc of L_6 on the boundary of d' , shown in Fig. 5-1. This roughness does not occur for higher values of the bifurcation parameter, b , for which the boundary of d' is smooth. The appearance of this arc gives the first *tongue*, a folding arc of a critical curve, creating roughness of the boundary. This roughness will increase as b continues to decrease, announcing the approach of a *contact bifurcation*.

FIGURE 5-1.

The absorbing area, shaded, and bounded by arcs of critical curves.

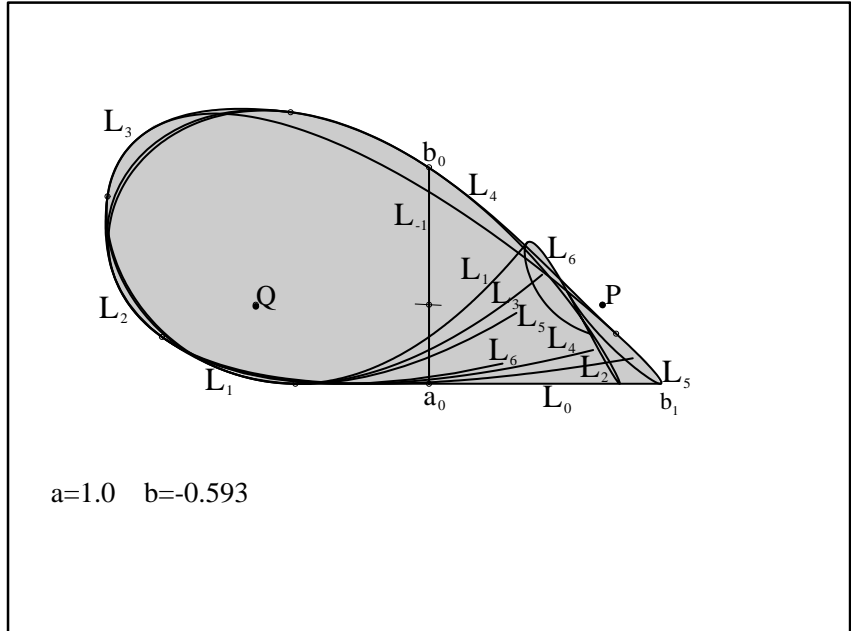


FIGURE 5-2.

The attractor, densely dotted by an actual trajectory.

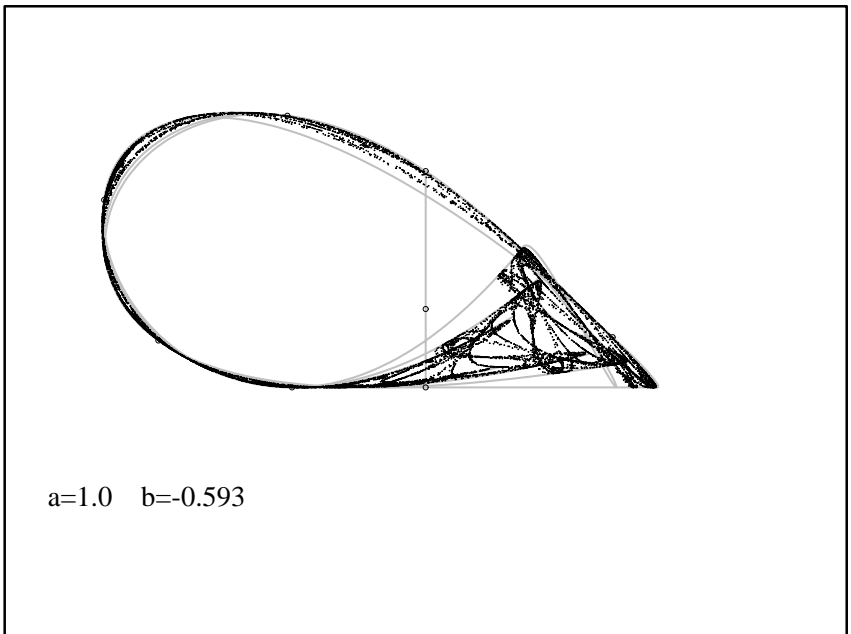


FIGURE 5-3.

With two new segments. The annular absorbing area, shaded, and bounded by arcs of critical curves, the images of these two segments.

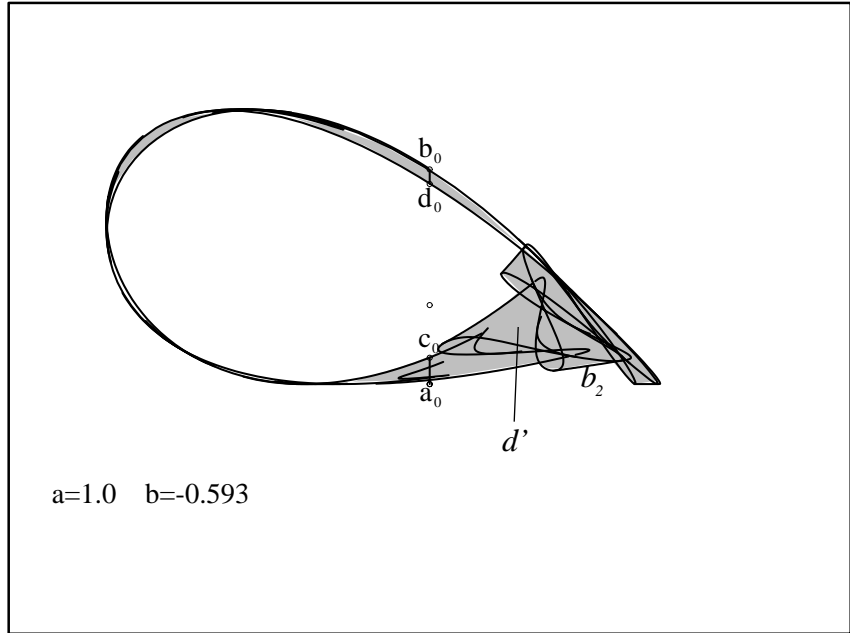


FIGURE 5-4.

An enlargement showing critical curves.

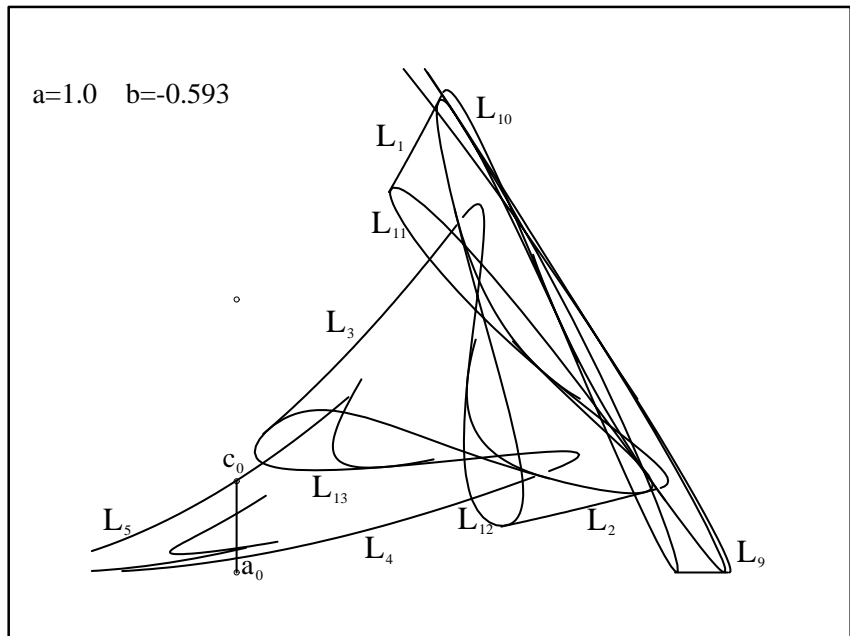


FIGURE 5-5.

An enlargement showing the attractor bounded by critical curves.

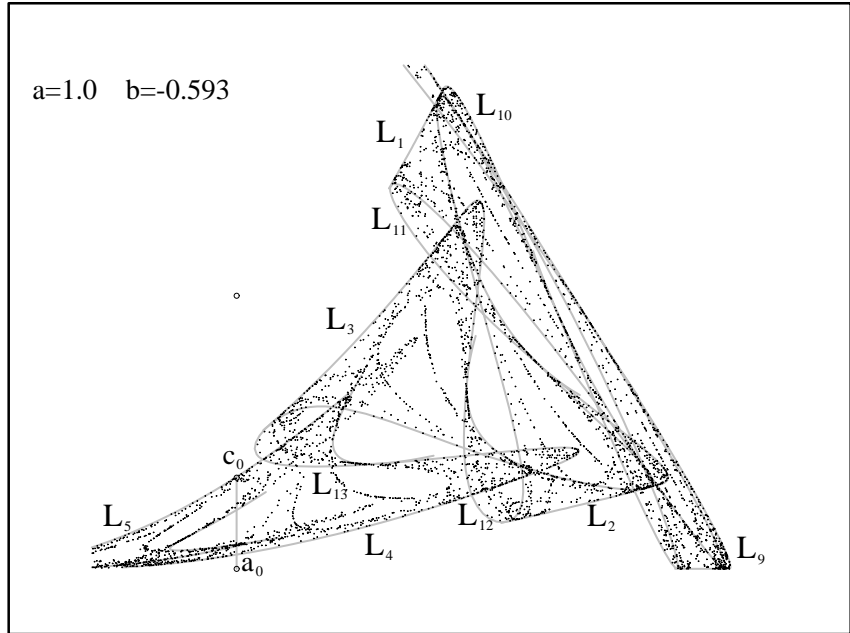
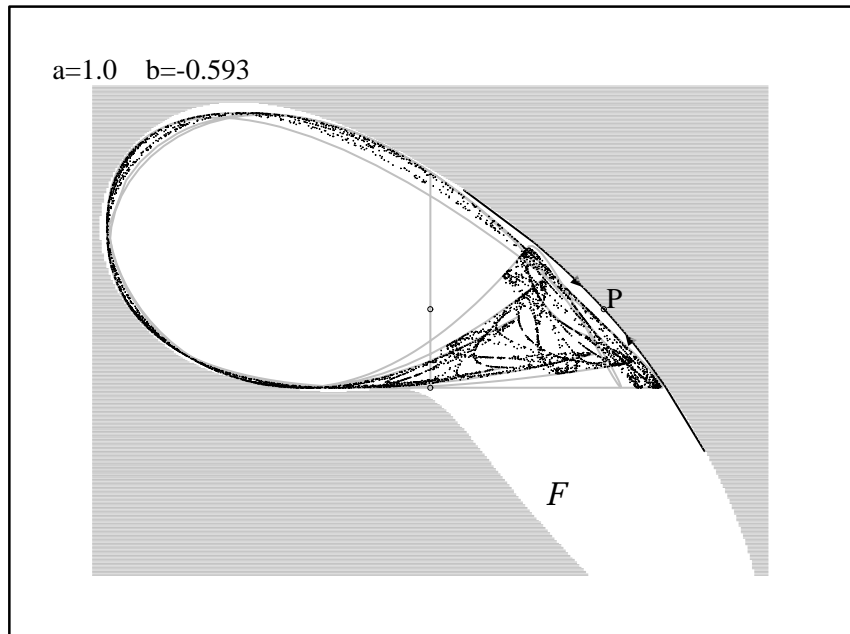


FIGURE 5-6.

The attractor in its basin, shaded.



Stage 2: $b = -0.59495$

This stage immediately precedes the first contact bifurcation, a type of bifurcation treated in more detail later, in Chapter 7. Figures 5-7 and 5-8, with 17 images of the segment $a_0 b_0$, show many tongues in the absorbing area, d' .

The chaotic set, d , contains only part of these tongues, as shown in Fig. 5-9. The tongues of the boundary of d' are approaching the inset of the saddle point, P , and thus the boundary of the basin $D(d')$. Note that d' is close to F in Fig. 5-9.

Figure 5-10 shows a smaller annular absorbing area, d'_a in d' , containing d . Figure 5-11 shows more detail. Figure 5-12 shows that d'_a , and d inside it, are still far from the frontier, F , of the basin of attraction.

FIGURE 5-7.

Six critical curves.

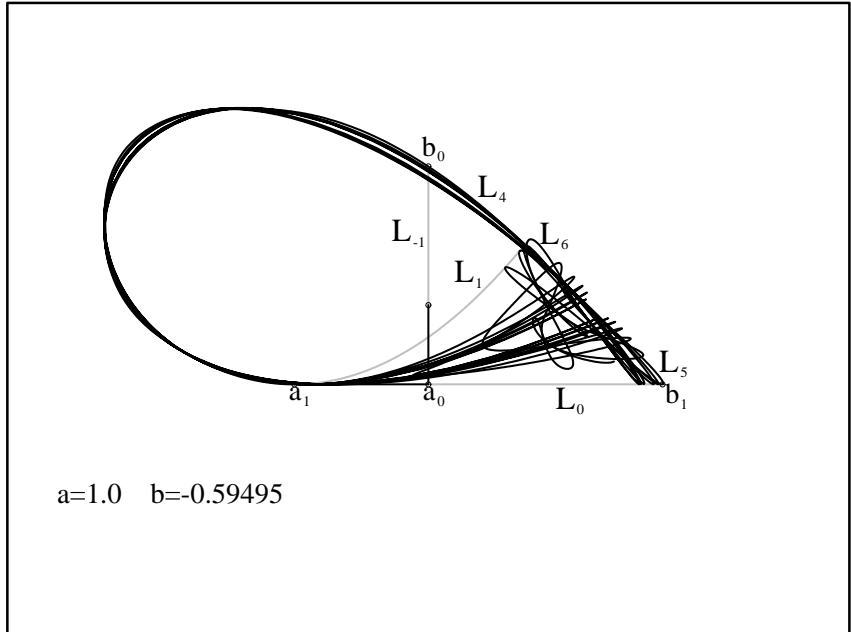


FIGURE 5-8.

Seventeen critical curves, enlarged, showing tongues.

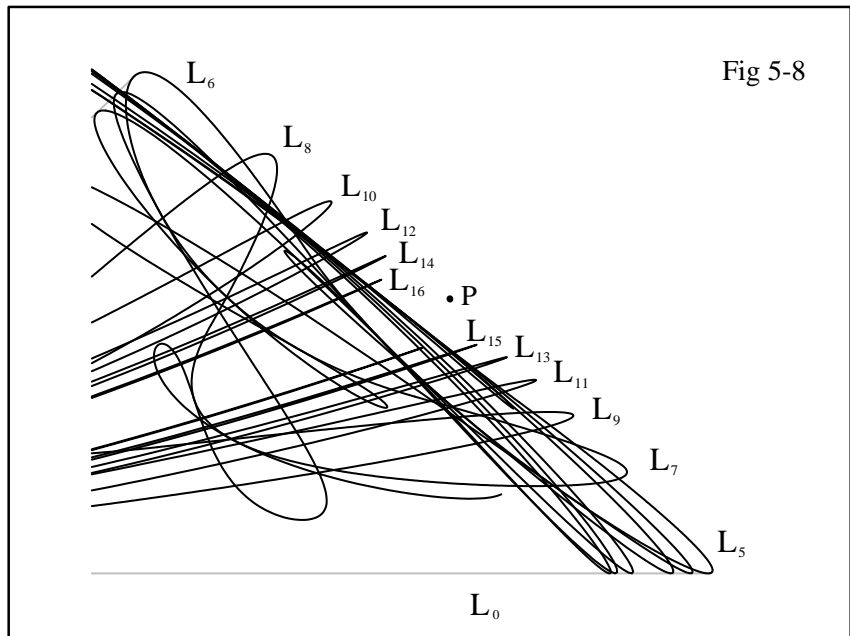


FIGURE 5-9.

The attractor, enlarged.

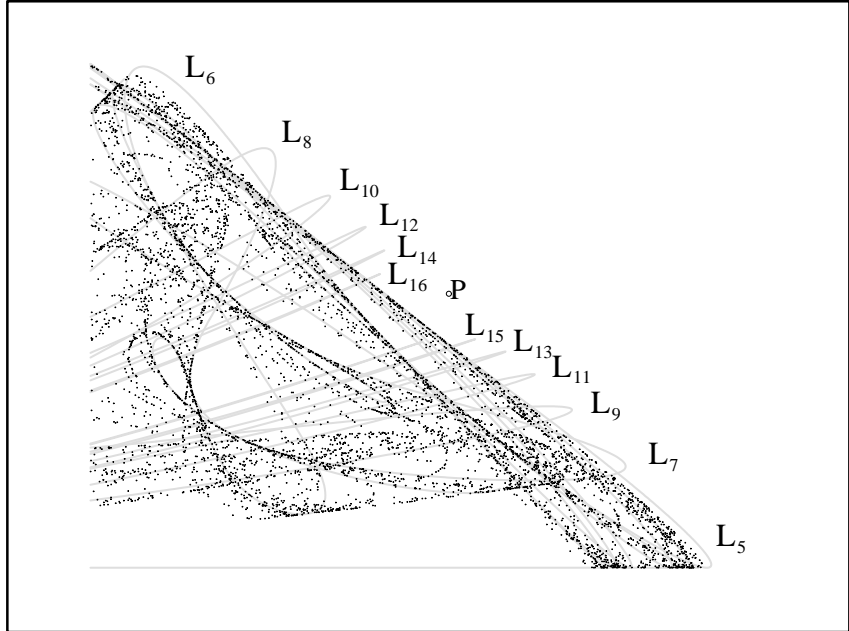


FIGURE 5-10.

The smaller annular absorbing area, defined by iterates of a reduced arc of a critical curve.

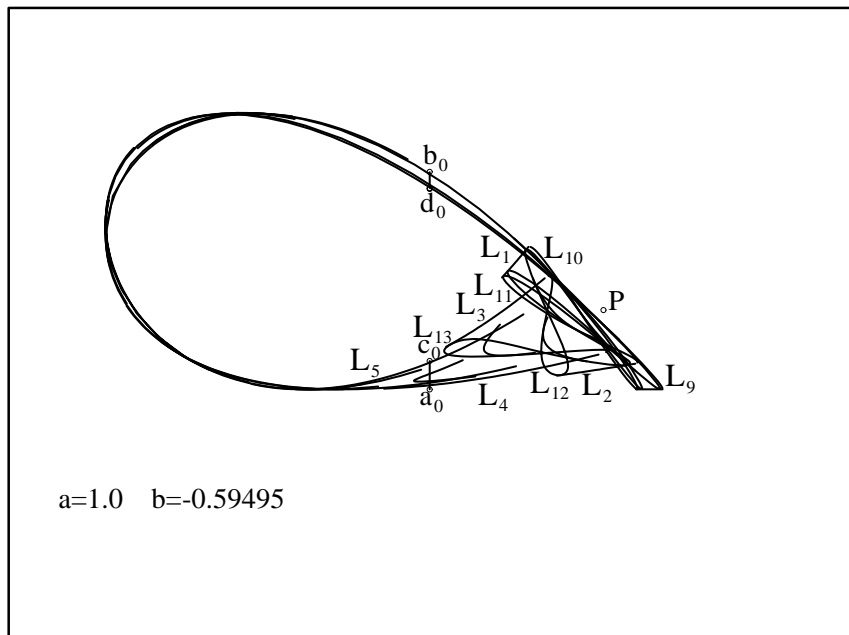


FIGURE 5-11.

An enlargement of the shorter critical arcs.

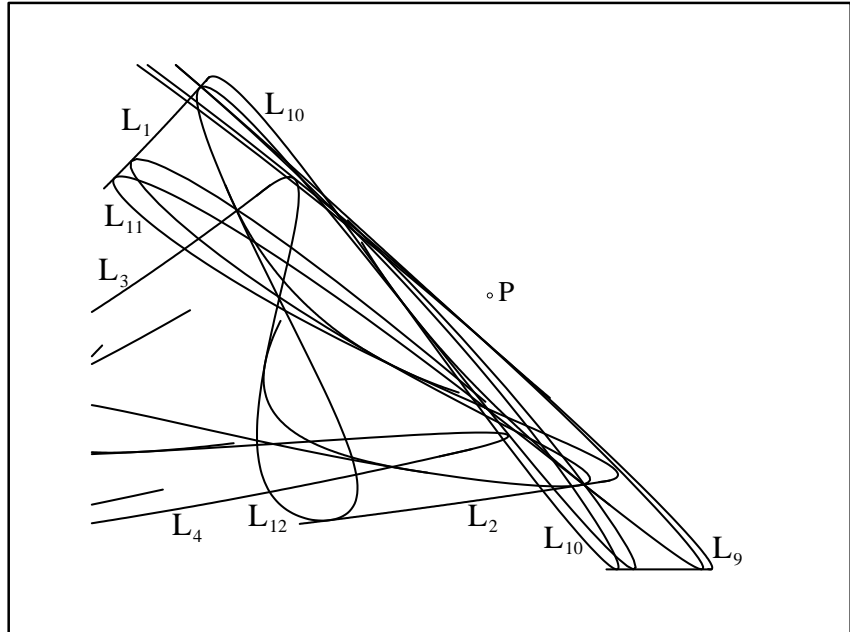
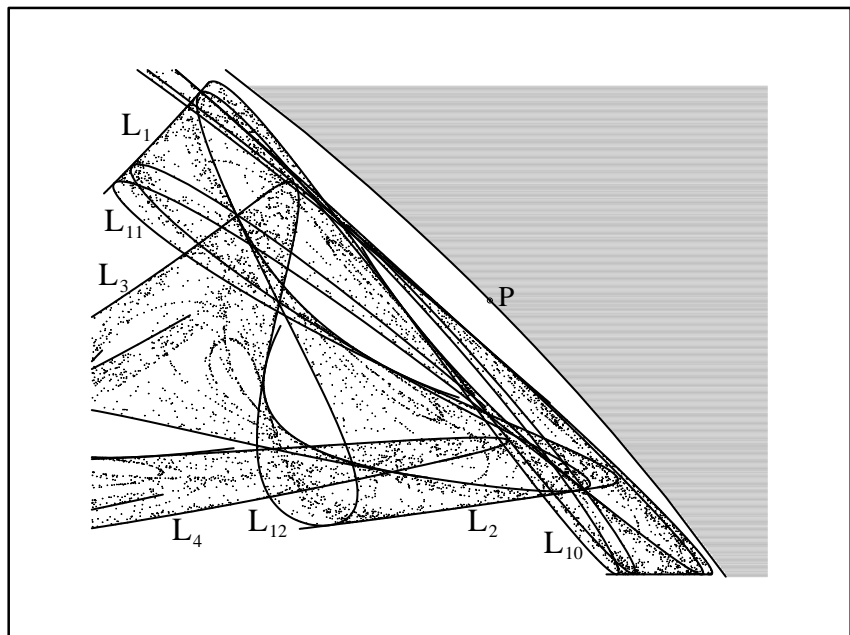


FIGURE 5-12.

A portion of the attractor and its basin, in the reduced annular absorbing area.



Stage 3: $b = -0.594962$

This stage is almost exactly the moment of the first contact bifurcation between the absorbing area, d' , and the frontier, F . Figure 5-13 shows that infinitely many tongues on the boundary of d' approach the fixed saddle, P , which lies on F . These tongues belong to images of the segment $a_{-1} a_0$ of L_{-1} . Thus we have a contact between the boundary of the absorbing area, d' and the boundary, F , of its basin, D . Figure 5-14 shows an enlargement near the fixed saddle.

In a further enlargement, Fig. 5-15, we see a point of contact, h_0 , between the boundary of d' and F . The iterates of this point converge to the saddle, P , as shown in Fig. 5-16. And at each of these image points, the images of the two boundaries are tangent; that is, the ends of the tongues are tangent to the inset of the saddle, P .

FIGURE 5-13.

The attractor,
among critical arcs.

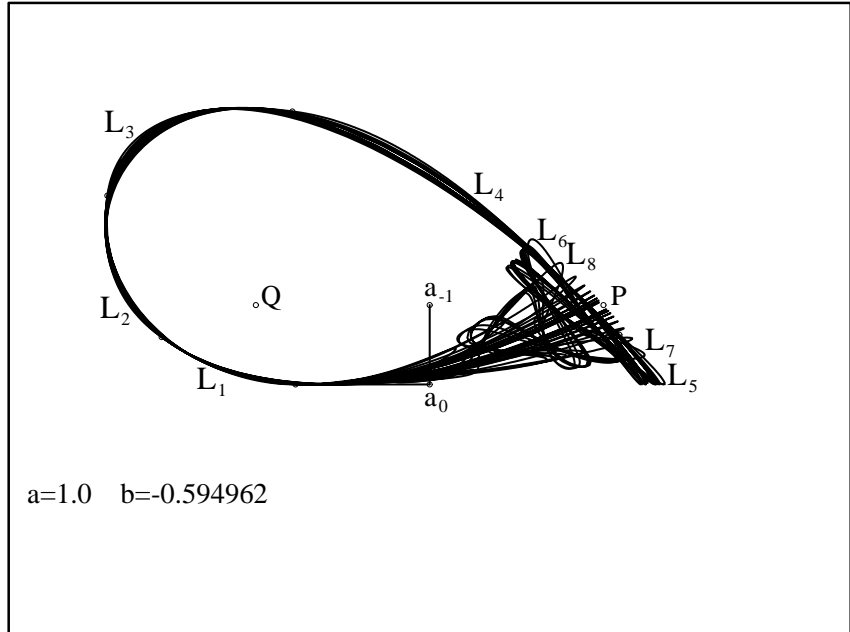


FIGURE 5-14.

An enlargement,
showing portions of
critical curves and
basin. Note the
tongues tangent to
the inset of P .

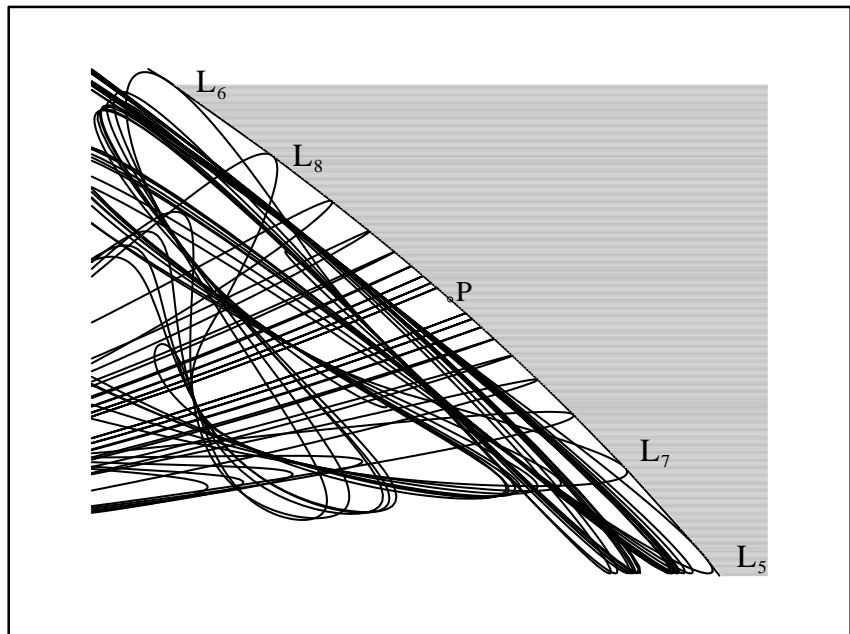


FIGURE 5-15.

Further enlargement, showing a point of tangency.

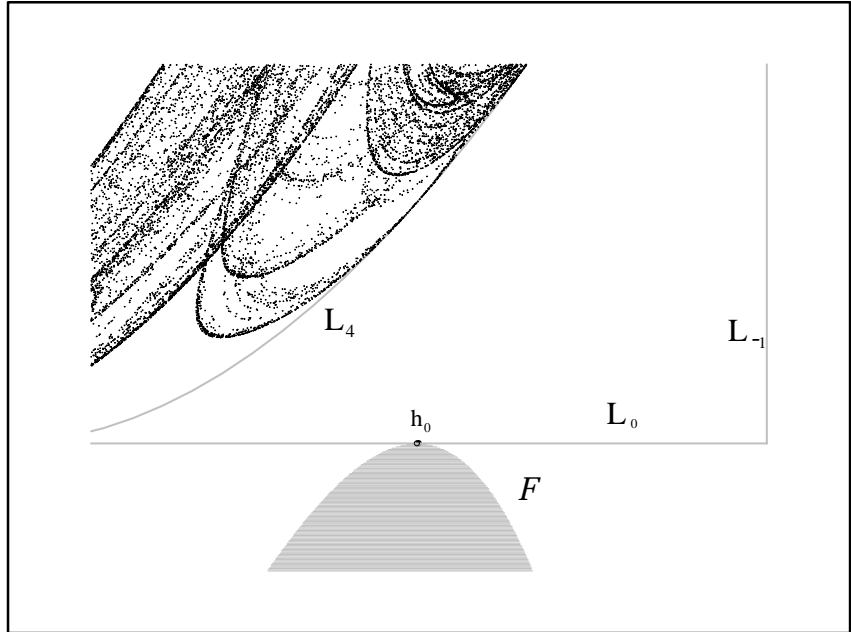
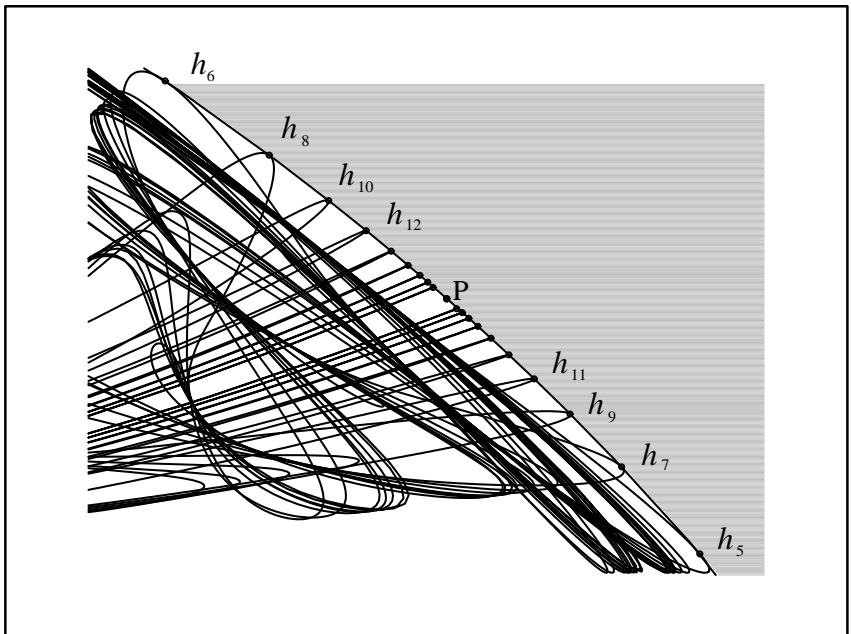


FIGURE 5-16.

Iterates of the point of tangency converging to P .



Stage 4: $b = -0.59500$

This stage is immediately after the first contact bifurcation. Figures 5-17 and 5-18, are made of 18 iterates of the segment $a_0 b_0$ of L_{-1} , where b_0 is the intersection of S_4 with L_{-1} (see Fig. 5-1). They show that some points of the tongues, having crossed through the inset of P separating the two basins, now are attracted to infinity. Thus, the area defined by Procedure 2 (see 4.3 above) is unbounded; infinite iterations are required to obtain an area which is absorbing. However, a smaller annular absorbing area, d'_a , containing d , may be constructed.

FIGURE 5-17.

Eighteen iterates of a critical segment.

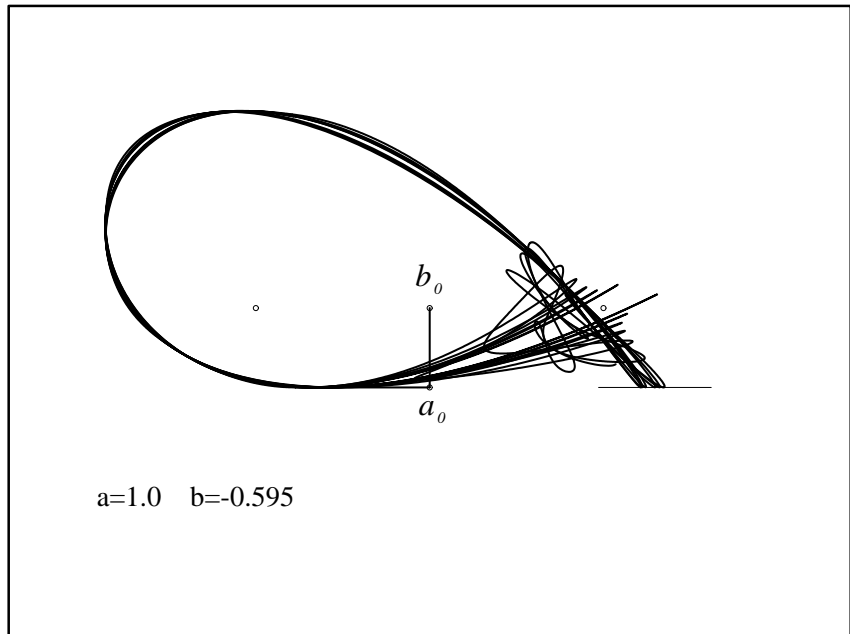
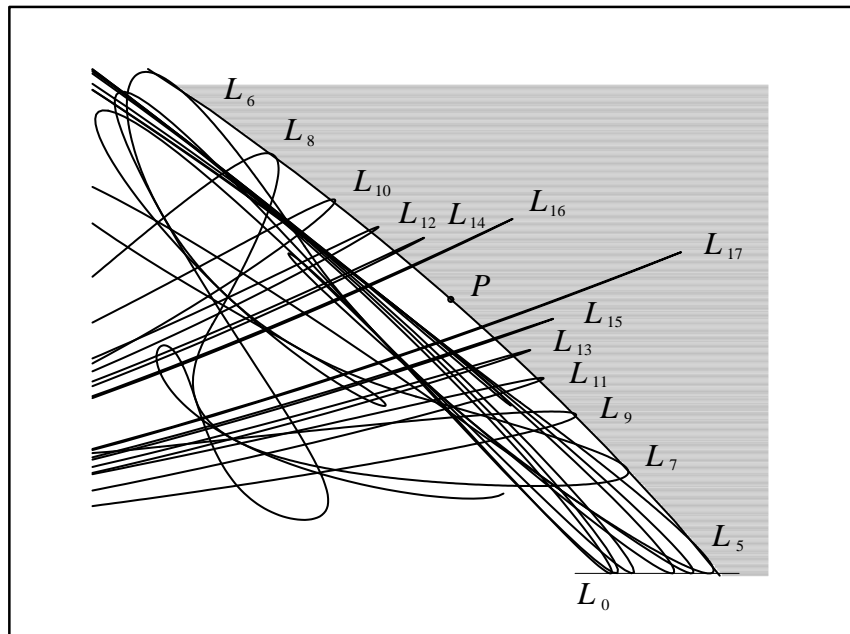


FIGURE 5-18.

Enlargement showing critical arcs and basin. Some tongues now cross the inset of P .



Stage 5: $b = -0.59520$

This stage is also just after the first contact bifurcation. Because the frontier, F , is the inset of the saddle point, P , it is invariant under the inverses of the map, by definition.

Figure 5-19 shows that after the first contact bifurcation, holes (such as those labelled H_{-1} , H_{-2}^1 , and H_{-2}^2) appear in the basin of attraction $D(d')$. These holes belong to the basin of infinity.

Note that topologically, the basin of infinity is not connected. It has disjoint pieces, which are holes of the basin of d' . And this basin is not simply connected, as it has holes which belong to the basin of infinity.

This is how the holes appear. After this first contact bifurcation, the frontier F crosses L , creating the sector H_0 bounded by F and L , as shown in the enlargement, Fig. 5-20. This sector constitutes a piece of the basin of infinity in the zone Z_2 . Since the sector H_0 belongs to the basin of infinity, so too do all of its preimages. One of these, H_{-1} , is shown as a small shaded hole in Figure 5-19. It is in the zone Z_2 . (The other, not shown, is in the zone Z_0 .) The shaded holes H_{-2}^1 and H_{-2}^2 are the two first-rank preimages of the hole H_{-1} .

The sector H_0 is bounded by an arc of F_e , and an arc of L having endpoints r_0 and s_0 . The first-rank preimage, H_{-1} , of the sector is composed of two areas joined by the arc $r_{-1}s_{-1}$ of L_{-1} . Thus H_{-1} is connected and it is a hole, as shown in Figs. 5-19 and 5-20. We regard this as a main hole. All other holes are preimages of a main hole, and they converge to the points Q and Q_{-1} .

We may regard F as the union of F_i and F_e , where F_i consists of the boundaries of all the holes, and F_e is the rest of the boundary of $D(d')$.

For further analysis of bifurcations involving contact of F and L , see BB. We will just describe some of the events in our present context. As b continues to decrease, the holes increase in size.

FIGURE 5-19.

The attractor and its basin.

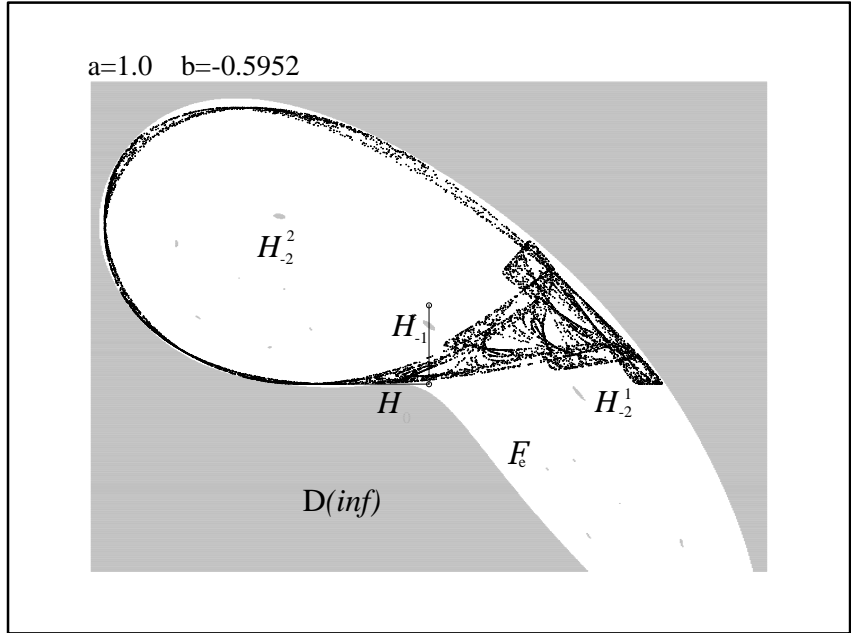
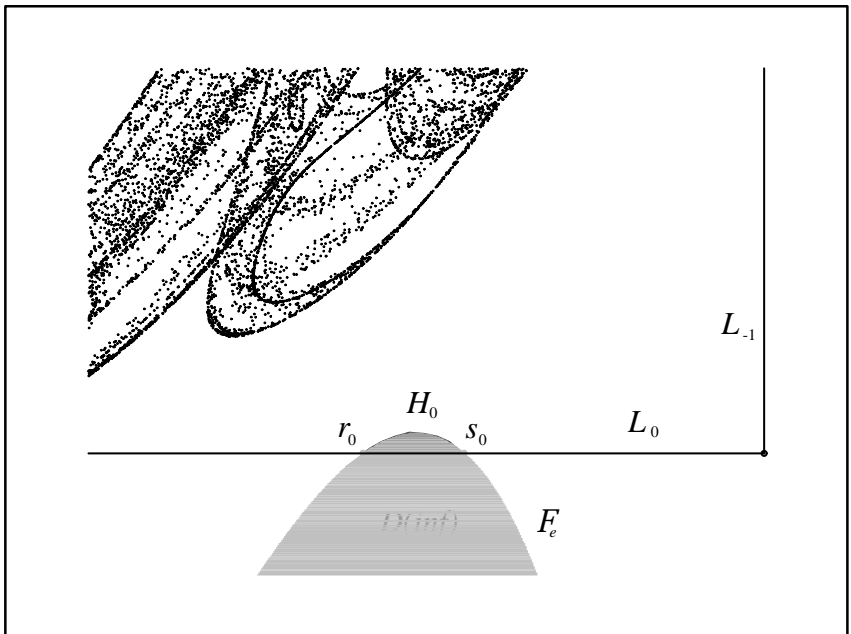


FIGURE 5-20.

Enlargement, showing the intrusion of the basin across the critical line. The domain of this enlargement is near the center of Fig. 5-19.



Stage 6: $b = -0.59600$

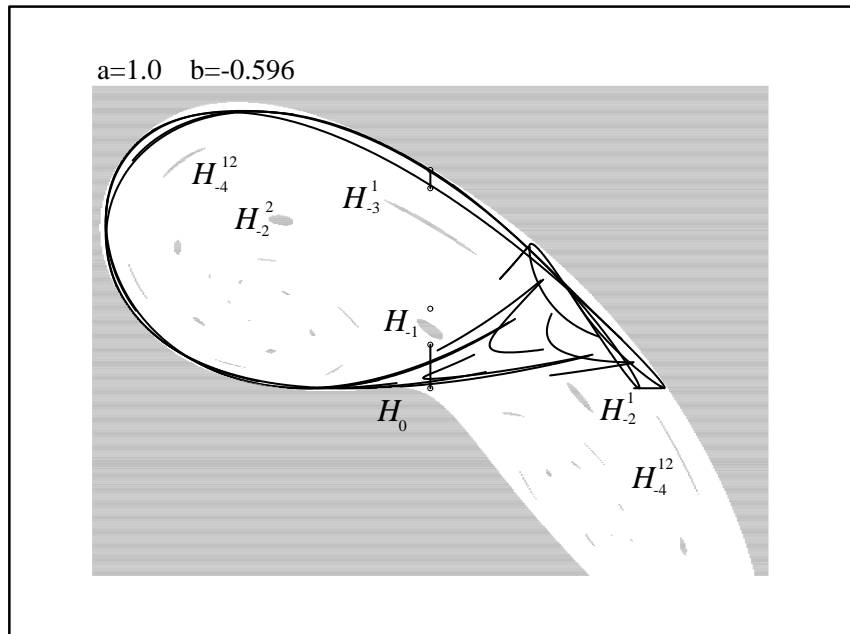
The preimage of H_{-1} (first-rank preimage of H_0) has two parts, and previously (when b was higher) one of them (denoted by H_{-2}^1) belonged to the region, Z_0 , of points having no preimage. But now, as b decreases further, this preimage becomes tangent to L , which is the frontier between Z_0 and Z_2 , and crosses through it into Z_2 .

This crossing is shown in Fig. 5-21. Thus a new set of holes is created, an infinite sequence of preimages of H_{-2}^1 disjoint from our previous system of holes. All these holes, old and new, get mapped eventually into the main hole, H_0 .

As b decreases further, the holes increase yet further in size.

FIGURE 5-21.

The holes grow larger.



Stage 7: $b = -0.59740$

In Fig. 5-22 we see the same holes as in the preceding stage, but they are wider. The hole H_{-4}^{11} , which belongs to the region Z_0 , is close to the critical curve, L .

See also the enlargement, Fig. 5-23.

FIGURE 5-22.

The holes are even larger.

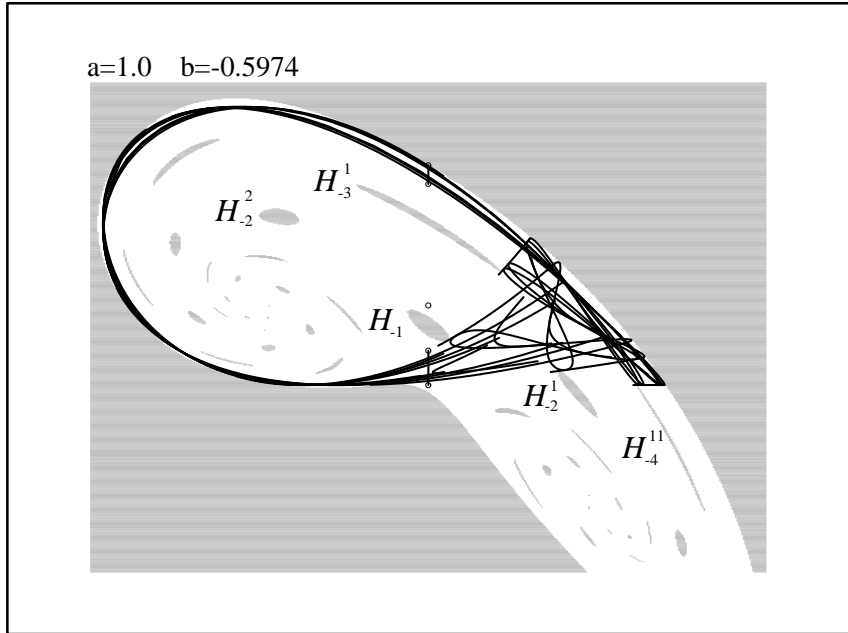
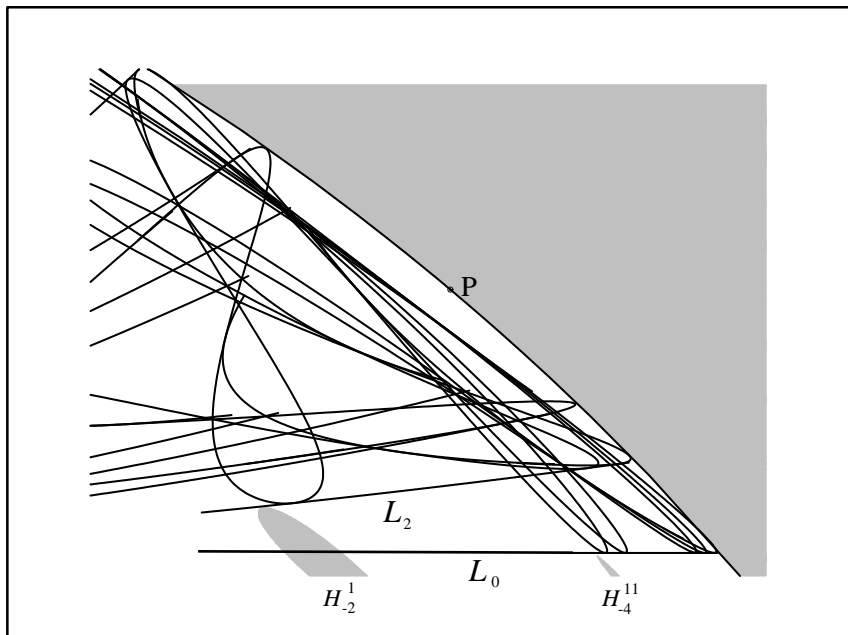


FIGURE 5-23.

An enlargement.



Stage 8: $b = -0.59800$

After further decreases in the parameter b , H_{-4}^{11} now intersects L , as shown in Fig. 5-24. Thus, we have passed another contact bifurcation, and we have a new system of holes, based on the hole H_{-4}^{11} .

In the enlargement, Fig. 5-25, we see part of H_{-4}^{11} in the zone Z_2^1 , and its image under two iterates of the map lies in the part of H_{-2}^1 above the critical curve, L_2 . At the recent contact bifurcation, when H_{-4}^{11} became tangent to L , H_{-2}^1 became tangent to L_2 , and H_{-1} became tangent to L_3 . Thus this contact bifurcation changed the topology (that is, the density of holes) of both the basin $D(d'_a)$, and its annular absorbing area, d'_a .

In Fig. 5-25, we see that the critical arcs of L_{10} , L_{11} , and so on, cross the frontier, F_e . Before the recent contact bifurcation, these arcs defined the boundary of an absorbing area. Notice also in Fig. 5-25 the hole \bar{H}_{-k} , a preimage of the new hole \bar{H}_{-4}^{11} which approaches the critical curve L from above, that is, from the zone Z_2 . Now a new absorbing area exists, and in Fig. 5-26 we see that its boundary includes arcs of L_{11} and L_{12} , without contacts with F_e .

FIGURE 5-24.

A new system of holes perforates the basin of our attractor.

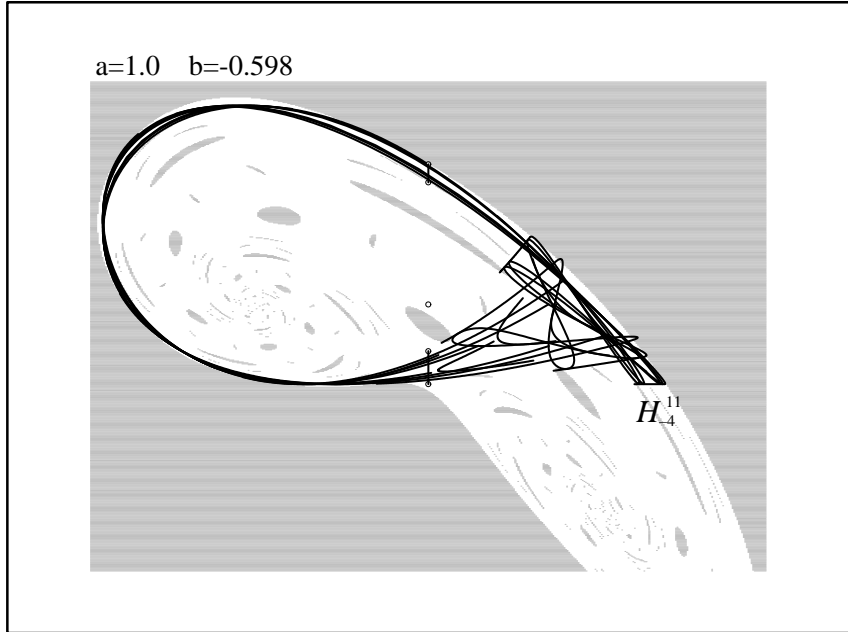


FIGURE 5-25.

Darker shading indicates the new tongues crossing into the basin of infinity.

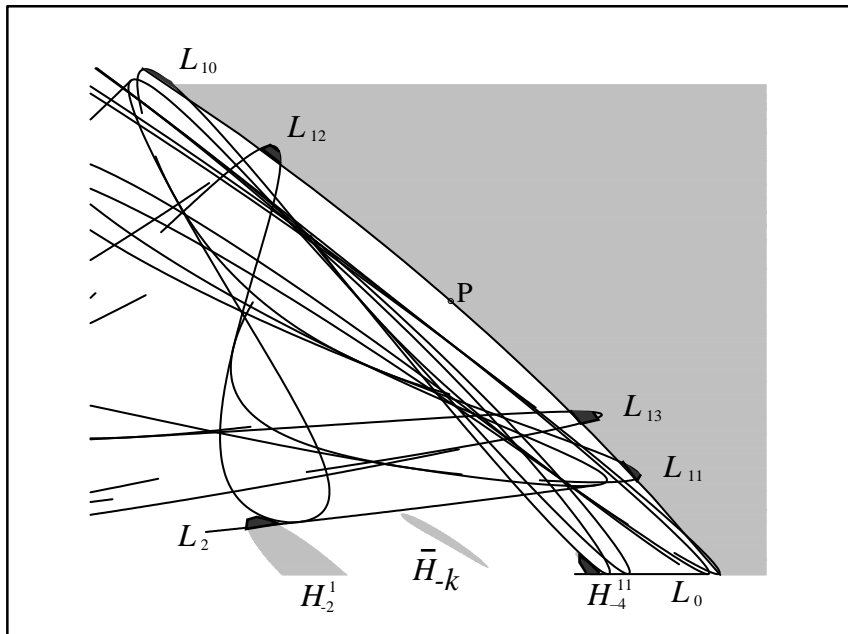
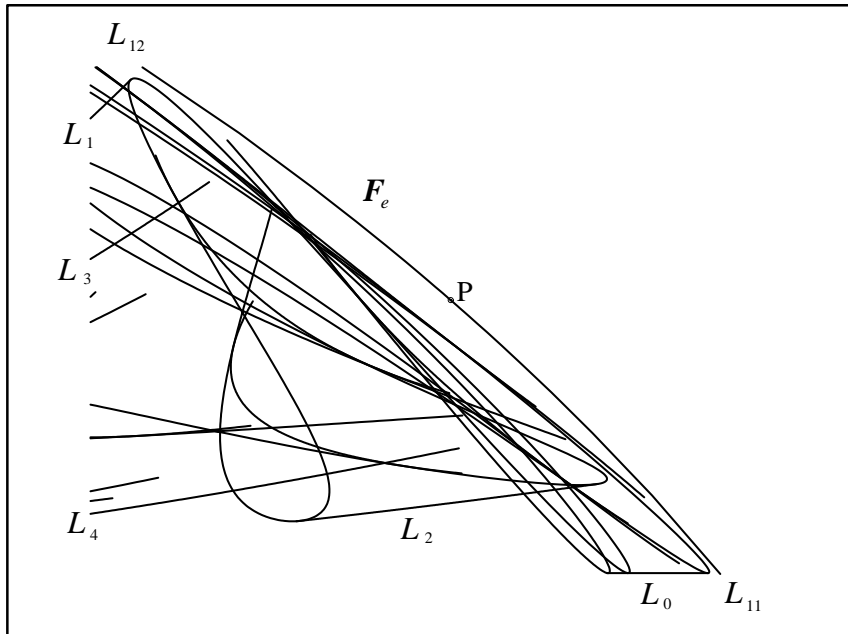


FIGURE 5-26.

The new absorbing area, bounded by these critical curves.

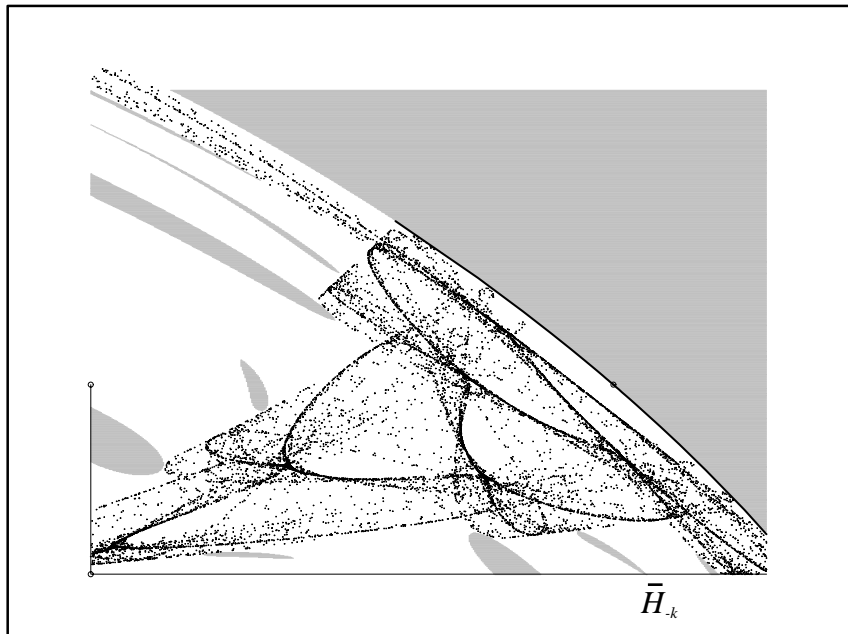


Stage 9: $b = -0.59820$

In Fig. 5-27, the hole \bar{H}_{-k} becomes tangent to L .

FIGURE 5-27.

The hole has descended to L from above.



Stage 10: $b = -0.59824$

In Fig. 5-28 the hole \bar{H}_{-k} crosses L . In this third contact bifurcation, we see holes rejoined, the inverse of the second contact bifurcation discussed in Stage 9. What had been two distinct holes (and their preimages) are now reunited, connected by a segment (and its preimages) in L_{-1} . This is marked “reunion” in Fig. 5-28, compare Fig. 5-24.

In the enlargements, Figs. 5-29 and 5-30, we can see images of critical arcs defining the boundary of the annular absorbing area, d'_a , and the chaotic area, d . Notice that the hole H_{-f} is in zone Z_0 , but is very close to L , which belongs to the boundaries of both d'_a and d . With further decreases of b , this hole makes contact with L . It may be established that such a contact will be the next contact bifurcation, but its effect will be different from the preceding ones.

FIGURE 5-28.

Some holes have now rejoined.

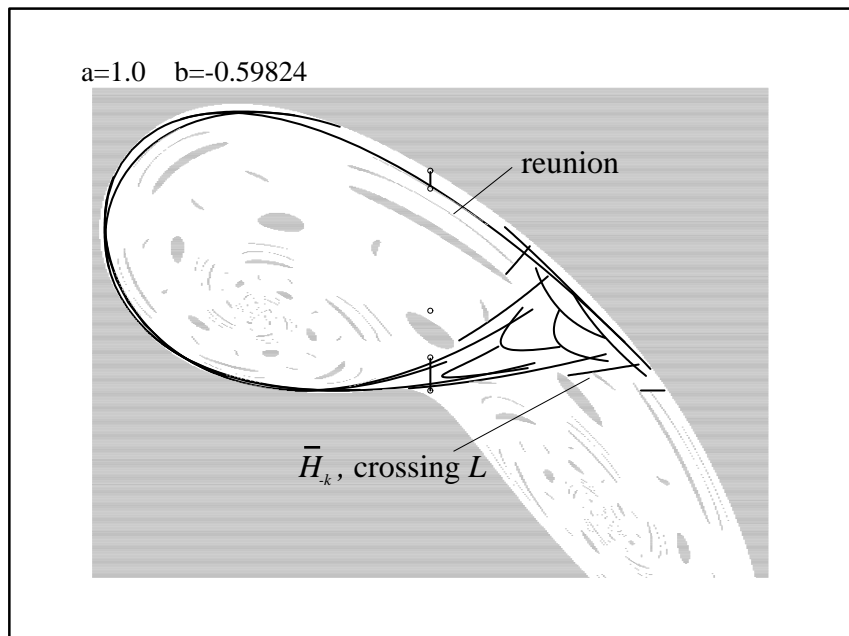


FIGURE 5-29.

Enlargement, showing the new holes below L in darker shading.

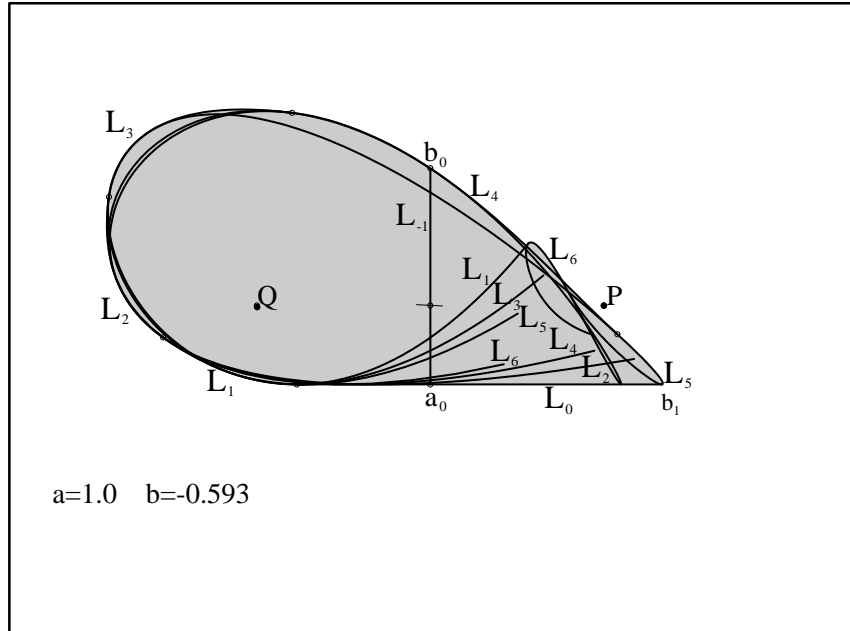
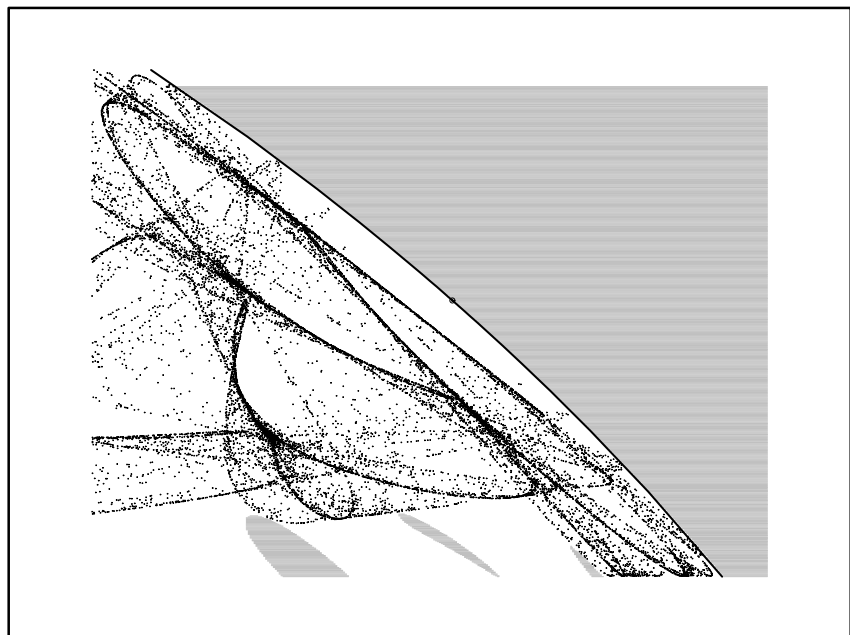


FIGURE 5-30.

Enlargement, showing the attractor and basin with holes.



Stage 11, $b = -0.598727$

This is the stage of contact predicted in Stage 10. The hole, H_{-f} , is tangent to L . The boundary F becomes tangent to the boundary of d at infinitely many points. These points comprise the trajectory of the point k_0 shown in Fig. 5-34. See Fig. 5-31, and its enlargements, Figs. 5-32 to 5-36.

The boundary of d has contact with the hole H_{-f} , as well as with all its images up to the main hole, and the sector H_0 and its images. These create the tangency of infinitely many tongues of d in the inset of P , as shown in Fig. 5-36. This is an example of *homoclinic tangency*: the tangency of the outset of the saddle point P to the inset of P . As the trajectory of this point of tangency tends to P in both future and past iterations, it is same-tending, or homoclinic, in the language of Poincaré.

The rank 1 preimage of the point k_0 is a point k_{-1} of L_{-1} within the chaotic area d (see Fig. 5-35). This tangency of the attractor and its basin boundary will cause an explosion of holes inside the chaotic area. We leave this to the interested reader to explore using the software ENDO, available through the companion CD-ROM.

The difference between this third contact bifurcation and those proceeding is that we have here a contact between the boundary of d , a chaotic area, and the boundary, F , of its basin. This contact causes the destruction of the chaotic area d , which is changed from an attractor to a repeller. The hole $H_{-(f+1)}$ (the preimage of H_{-f}) possesses an arborescent sequence of preimages inside the chaotic area, d , leaving a chaotic repeller. Nearby trajectories are now attracted to other attractors, at infinity.

FIGURE 5-31.

The third contact bifurcation.

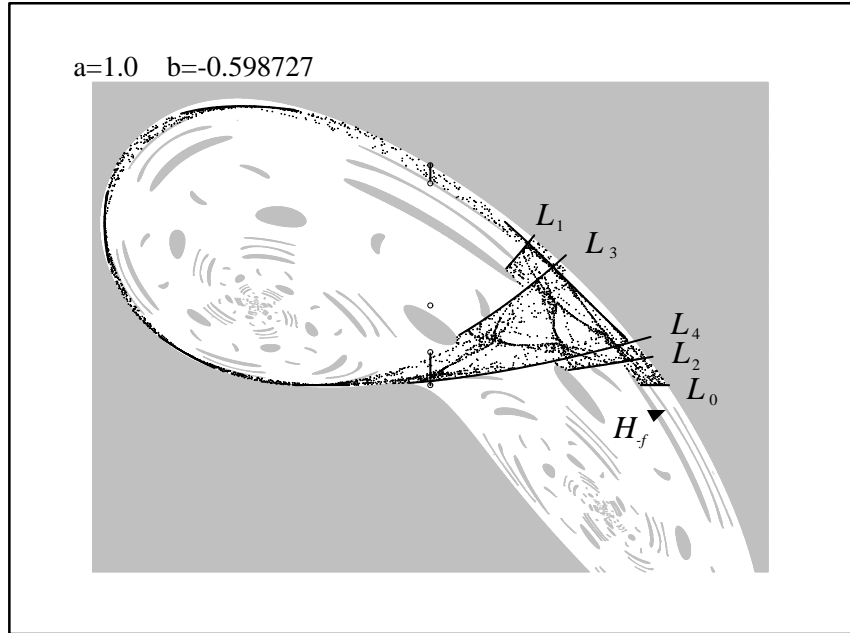


FIGURE 5-32.

Enlargement of a rectangle near the center of Fig. 5-31.

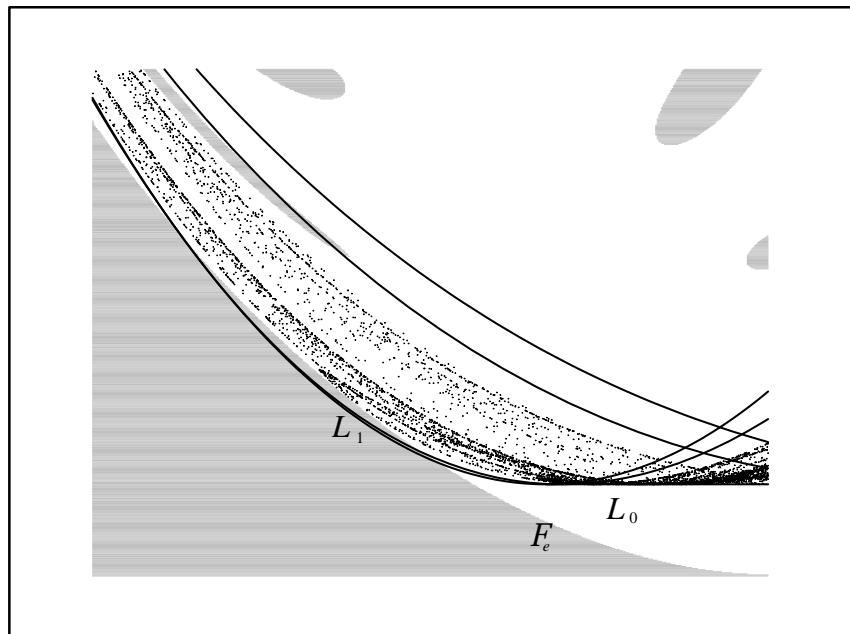


FIGURE 5-33.

The basic hole.

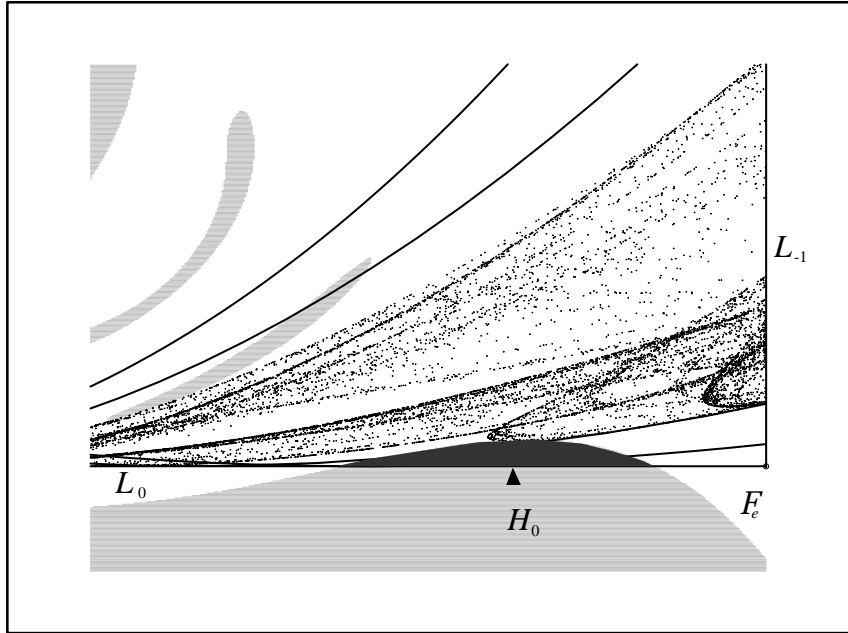


FIGURE 5-34.

The point of contact.

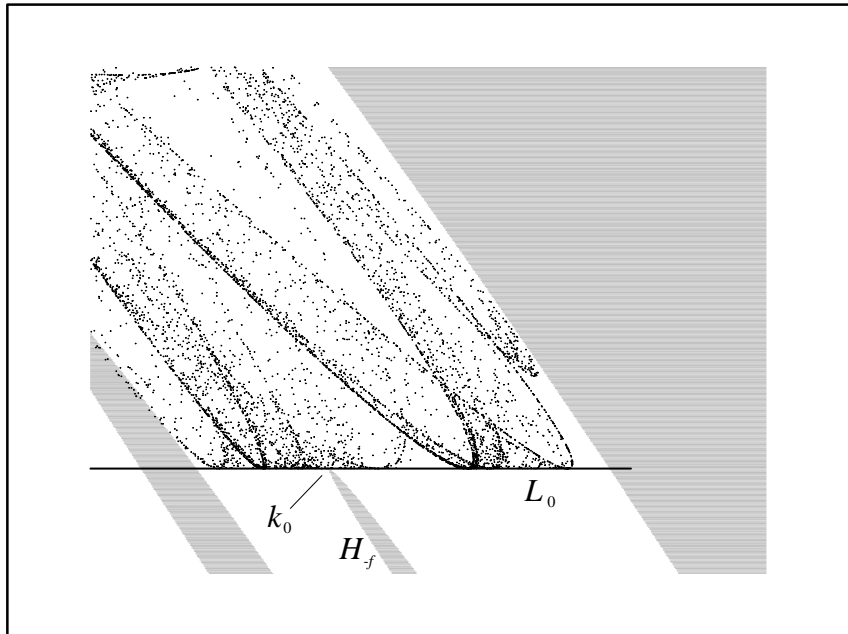


FIGURE 5-35.

A preimage of the point of contact.

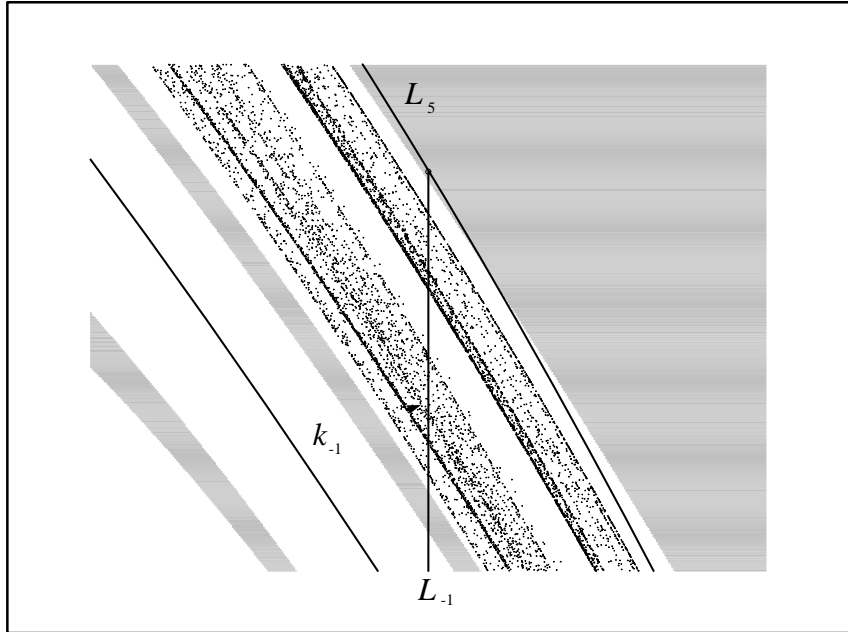


FIGURE 5-36.

Many contacts of the boundary of the chaotic area and the boundary of its basin.

